Experimental analysis of the forming behavior of uni- and bidirectional non-crimp fabrics for different geometries

Bastian Schaefer, Ruochen Zheng, Julien Colmars, Auriane Platzer, Naïm Naouar, Philippe Boisse, Luise Kaerger

Composites Part B 287 (2024) 111765

Contents lists available at ScienceDirect

Composites Part B

journal homepage: www.elsevier.com/locate/composites

Experimental analysis of the forming behavior of uni- and bidirectional non-crimp fabrics for different geometries

Bastian Schäfer [a,1,*], Ruochen Zheng [b,1], Julien Colmars [b], Auriane Platzer [b], Naim Naouar [b], Philippe Boisse [b], Luise Kärger [a]

[a] Karlsruhe Institute of Technology (KIT), Institute of Vehicle System Technology (FAST), Lightweight Design (LB), Karlsruhe, 76131, Germany
[b] INSA Lyon, CNRS, LaMCoS, UMR5259, Villeurbanne, 69621, France

ARTICLE INFO

Dataset link: Forming tests of a uni- and a bidirectional non-crimp fabric for different orientations and geometries (hemisphere, tetrahedron, square box) (Original data)

Keywords:
A. Fabrics/textiles
A. Unidirectional non-crimp fabric
A. Bidirectional non-crimp fabric
E. Forming

ABSTRACT

For efficient large-series production and improved process design, a profound understanding of a textile's forming behavior is crucial to ensure adequate drapability and defect-free components. Woven fabrics have often been the focus of research due to their easier formability, while non-crimp fabrics (NCFs) have been investigated much less despite their higher lightweight potential, resulting in a limited experimental basis for the validation of numerical models. Therefore, forming experiments of a unidirectional and a bidirectional NCF are conducted for different configurations and punch shapes, including hemisphere, tetrahedron, and square box. The macroscopic strains are captured throughout the entire process using digital image correlation (DIC) and comprehensively analyzed in combination with the outer contour and resulting defects. Fundamental differences in the deformation behavior of both textiles are identified. For the balanced Biax-NCF, the tricot stitching couples the deformation of both fiber layers and the fabric mainly deforms under symmetrical shear with limited yarn slippage or defects. For the highly unbalanced UD-NCF, the lack of a second fiber direction results in an asymmetrical deformation behavior. The UD-NCF deforms due to shear parallel to the fiber yarns superimposed with transverse tensile and compressive strains in different deformation modes. The data generated in this study is freely available at https://doi.org/10.5281/zenodo.12516897.

1. Introduction

Carbon fiber reinforced composites (CFRP) are utilized in various industries such as aeronautic and automotive, due to their exceptional weight-specific stiffness and strength, as well as their potential for integral design [1–3]. Thereby, non-crimp fabrics (NCFs) provide the highest lightweight potential among available textile reinforcements. Their specific architecture consists of one (UD-NCF), two (Biax-NCF) or more overlapping layers of unidirectional plies of continuous fibers bonded by intricate stitching, effectively avoiding any weakening undulations.

Liquid composite molding processes are one option to manufacture high-performance composites [4,5]. Thereby, fabric forming is a key manufacturing step in which an initially flat stack of fabric is shaped into a complex 3D shape and undergoes large deformations [6]. The large deformations determine the final fiber orientation and directly impact the reinforcement's permeability as well as mechanical properties of the finished components. However, NCFs are more susceptible to forming defects like inter-yarn gap formation (gapping), yarn slippage and fiber waviness compared to woven fabrics [7–11]. To optimize the molding process and prevent defects, a profound understanding of the fabric's forming behavior is crucial. For the investigation of forming behavior, detailed tests are often performed first on simplified geometries representing the most challenging features of more complex components, like double-curved surfaces or various radii of edges and corners. Woven fabrics have often been the focus of research on textile forming due to their better formability [6,9,12–14], while NCFs [9,15–17] and especially UD-NCFs have been investigated much less [10,11,18–20].

The *hemispherical* punch is the most common shape and is often used for studying the formability of woven fabrics [21–24], as well as NCFs [10,16,18,25]. It is a rather simple double-curved geometry that still imposes significant in-plane shear deformation. Bel et al. [15] analyzed and measured sliding between fiber plies in a Biax-NCF for this shape. Schirmaier et al. [18] and Ghazimoradi et al. [10] observed

* Corresponding author.
E-mail addresses: bastian.schaefer@kit.edu (B. Schäfer), ruochen.zheng@insa-lyon.fr (R. Zheng), julien.colmars@insa-lyon.fr (J. Colmars), auriane.platzer@insa-lyon.fr (A. Platzer), naim.naouar@insa-lyon.fr (N. Naouar), luise.kaerger@kit.edu (L. Kärger).
[1] Authors Bastian Schäfer & Ruochen Zheng contributed equally to this work.

https://doi.org/10.1016/j.compositesb.2024.111765
Received 22 May 2024; Received in revised form 22 July 2024; Accepted 13 August 2024
Available online 17 August 2024

notable gapping due to the low stiffness of the stitching and wrinkling parallel to the fiber yarns for a UD-NCF in hemisphere tests.

The *tetrahedral* punch was developed to represent a slanted corner of more complex components and provoke higher shear angles as well as the formation of out-of-plane defects [12,26–28]. Viisainen et al. [28] compared the hemisphere and tetrahedron for a ±45°-Biax-NCF and found similar types of wrinkles as well as deformation modes for both shapes, but significantly higher shear angles and severity of the wrinkles for the tetrahedron test.

The *square box* punch is commonly used for metal forming analysis [29,30], but few researchers have shown its capability to induce very high shear angles for textile reinforcements [22,24,31–33]. Bai et al. [34] compared a large variety of woven fabric architectures as well as some multiaxial NCFs in box tests and identified a strong correlation between a fabric's membrane-to-bending stiffness ratio and the formation of wrinkles.

The deformation behavior and the formation of defects in forming tests can be analyzed through various measurements. The outer contour of the blank after forming gauges the material draw-in, allows conclusions about the symmetry of the deformation behavior, and is frequently used for the validation of forming simulations [22,23,27,35,36]. The measurement of global and local strains is accomplished by a variety of different methods. Many researchers utilize point-wise measurements to determine shear angles, as in-plane shear is a primary deformation mode of most balanced fabrics [12,23,24,36,37]. In these approaches, grids are reconstructed from local markers on the fabric or images are analyzed to locally measure the angle between visible fiber directions. However, these methods are not suitable for NCFs, since significant yarn slippage as well as transverse tensile and compressive strains occur superimposed to shear deformation [10,19,38]. Alternatively, different DIC methods are utilized to measure the 3D geometry and full strain field of the deformed fabric. However, those methods require either the possibility to remove the fabric from the mold without further deformation [17,35,39–41], or specialized stereo camera systems in combination with an open die [10,28,33,42].

The objective of this paper is to investigate the forming behavior and improve the understanding of the occurring membrane deformation modes of a UD- and Biax-NCF using various punch shapes and layup configurations. This study focuses on the membrane behavior, since in addition to shear deformation, significant transverse tensile and perpendicular compressive strains as well as fiber slippage are observed for NCFs. However, their relevance during forming has rarely been quantitatively investigated, as previous studies have mainly focused on the shear angle or out-of-plane wrinkling. The outer contour of the fabric after forming is analyzed to compare the general deformation behavior of both UD- and Biax-NCFs. A transparent die in combination with an open-source DIC-method is applied to measure the global and local strains throughout the entire draping process, without removing the dry fabric or application of a specialized camera system. Furthermore, distinct forming defects and their typical locations are presented and discussed. In addition, comprehensive quantitative results are generated for future validation of numerical models, because these are very sparsely available for NCFs, especially for UD-NCF.

2. Material

In this study, a unidirectional (UD300) and bidirectional (MD600) non-crimp fabric (NCF) both without binder are used, cf. Fig. 1. The fabrics are manufactured by Zoltek™ and produced from their PX35-50K continuous carbon (CF) fiber heavy tows. Both fabrics are stitched together with a 76 dtex Polyester stitching yarn in a Tricot pattern. A textile layer of UD300 consists of a single fiber layer of aligned CF tows in warp direction with thin glass fibers (GF) in weft direction on the back for improved handleability. A textile layer of MD600 comprises two fiber layers in a 0°/90° orientation. Both fabrics have a similar number of CFs in each fiber layer with about $300\,\mathrm{g\,m^{-2}}$ in their respective reinforcing directions.

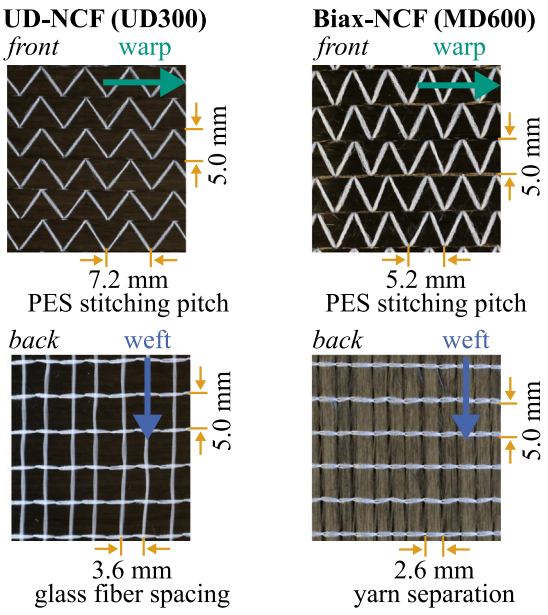

Fig. 1. (a) Unidirectional NCF (UD300) and (b) bidirectional 0°/90°-NCF (MD600).

3. Experimental test setup and procedure

3.1. Experimental setup

The platform developed for the experimental forming tests is shown in Fig. 2.

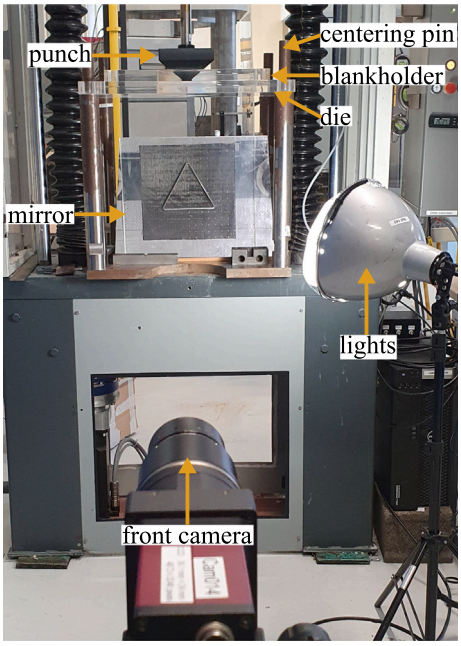

Fig. 2. Experimental setup of the forming tests.

This platform consists of two modules: a mechanical module, housing the motion control system, punch, blank holder, and die for generating displacement and applying pressure; and an optical module, comprising cameras, mirror and lights for measurements. The blank holders apply their own weight to the fabric, and centering pins prevent any in-plane movement. The platform has been successfully used in previous studies to investigate the forming behavior of woven fabrics

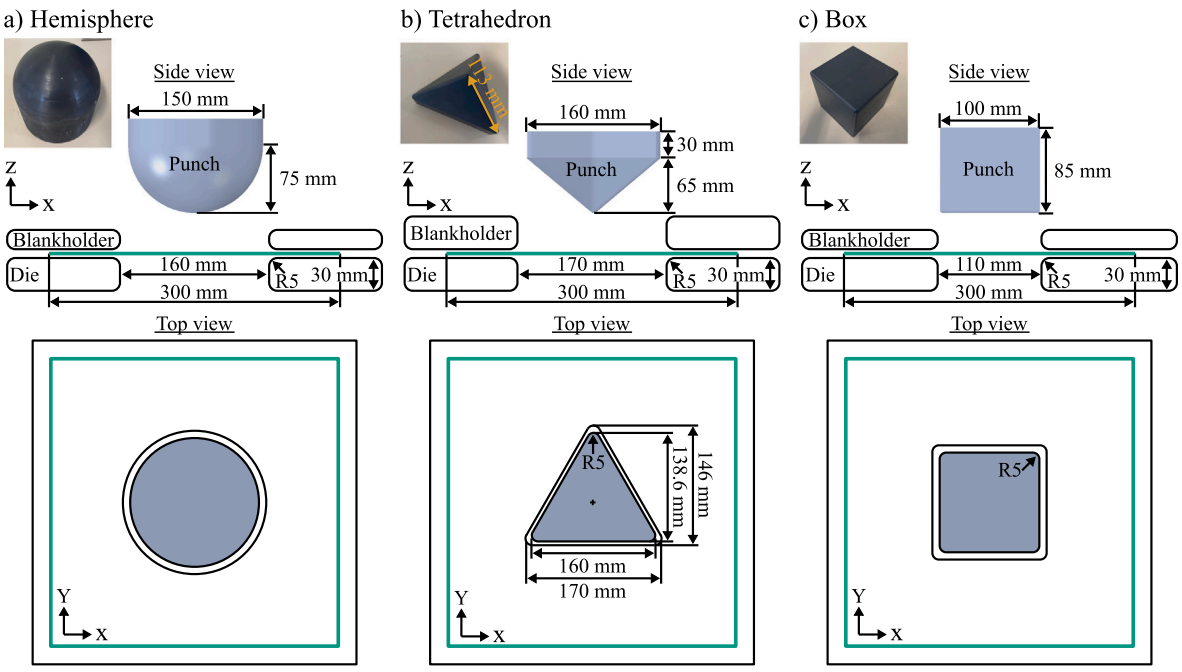

Fig. 3. Schematics and dimensions of the utilized shapes: (a) Hemisphere, (b) tetrahedron and (c) box.

and subsequently validate macroscopic models [23,24,31]. The experimental setup is mounted to a universal testing machine by ZwickRoell. The blank holder and die are made of transparent methyl methacrylate (PMMA) to allow for the acquisition of digital images by the optical module. The mirror is positioned at a 45° angle at the base, allowing the camera to capture images from its reflection. A top-mounted camera is connected to the horizontal beam on the machine to capture images of the rear side.

Three types of punches (hemisphere, tetrahedron, and square box) along with their corresponding shapes of blank holder and die are utilized in this study. Their dimensions and schematic are displayed in Fig. 3. The forming depths are 75 mm, 95 mm, and 85 mm with blank holder weights of 1.7 kg, 6.0 kg, and 1.7 kg for the hemisphere, tetrahedron, and square box punches, respectively. The thickness of the transparent lower dies is 30 mm.

The utilized specimens of UD- and Biax-NCF are from the same roll of material with dimensions of 300 mm × 300 mm, which were precisely cut on an automated cutting table by Zünd Systemtechnik AG, Altstätten, Switzerland. The specimen size was chosen based on previous studies with woven fabrics [23,24,31] without further optimization of its effect on the deformation in the center. To investigate the impact of yarn orientation and multiple layers on the material's deformation, three types of single-layer ($[0°_U]$, $[45°_U]$, $[90°_U]$) and two types of double-layer($[0°_U/45°_U]$, $[0°_U/90°_U]$) configurations of UD-NCF and two types of single layer ($[(0°/90°)_B]$, $[(\pm45°)_B]$) and one type of double-layer $[(0°/90°)_B/(\pm45°)_B]$ configurations of Biax-NCF were used in the forming tests. Each configuration was repeated three times for each configuration of UD-NCF, and at least twice for Biax-NCF due to the lower variability.

3.2. Macroscopic strain measurement method

The yarn deformation is measured via Digital Image Correlation (DIC) with a regular grid of white dots of acrylic paint using a stencil with a distance of $l_e = 10$ mm, as shown in Fig. 4 a. In a previous study, the same procedure was employed for an analysis of the membrane behavior of the same UD- and Biax-NCF in off-axis-tension tests [38], revealing a slight influence of the applied dot pattern on the measured forces, but a negligible influence on the deformation. The regular grid was applied to only half of the specimen to allow a direct comparison with the unmarked specimen under the same conditions. Again, a negligible influence of the dot pattern was observed in all tests.

The displacement of each dot was tracked with an open-source MathWorks Matlab DIC tool [43], which was already successfully applied in characterization tests for draping by Pierce et al. [44] and Schirmaier et al. [18,19]. Subsequently, four dots are combined into a 2D quadrilateral element and the deformation gradient $\boldsymbol{F}$ rotated in the initial fiber direction is calculated based on linear shape functions [45].

During the tests, especially for UD-NCF, large shear strains superimposed with transverse tensile deformation in the stitching direction and compression perpendicular to the carbon fiber yarns are expected on a macroscopic level [19,38,46]. Therefore, in addition to the components of the Green–Lagrange strains E_{11} and E_{22} representing the quadratic stretches along the principle directions **a** and **b** respectively, two other strain measures are tracked. First, the shear angle γ_{12} is calculated according to

$$\gamma_{12} = \frac{\pi}{2} - \psi_{12} = \frac{\pi}{2} - \arccos\left(\frac{C_{12}}{\sqrt{C_{11}}\sqrt{C_{22}}}\right), \tag{1}$$

where ψ_{12} is the current angle between the principle directions (**a** and **b**) and $\boldsymbol{C}$ is the right Cauchy–Green tensor. Second, the perpendicular stretch $E_\perp$ in the derived direction $\mathbf{b}^\perp$ which is the component of **b** that remains perpendicular to the carbon fiber direction **a**

$$E_\perp = \sqrt{2\,E_{22}+1}\,\sin(\psi_{12}) - 1. \tag{2}$$

Directions **a**, **b** and $\mathbf{b}^\perp$ are defined based on the principle material directions $\mathbf{a}_0$, $\mathbf{b}_0$ and $\mathbf{b}_0^\perp$ as shown in Fig. 4 b. Initially, $\mathbf{a}_0$ is aligned with the visible carbon fiber yarns in warp direction and $\mathbf{b}_0$ is aligned with the weft direction, cf. Fig. 1, which coincides with the second fiber direction for Biax-NCF and the thin glass fibers for UD-NCF.

These strain measurements allow distinction between different deformation modes, cf. Fig. 4 (d), which are observed during characterization for the investigated UD- as well as Biax-NCF [38]. In the case of pure shear, E_{22} is zero and thus $E_\perp$ is directly coupled to γ_{12}, cf. Eq. (2), while both strains are independent of each other for mixed deformation modes. The perpendicular strain quantifies the distance

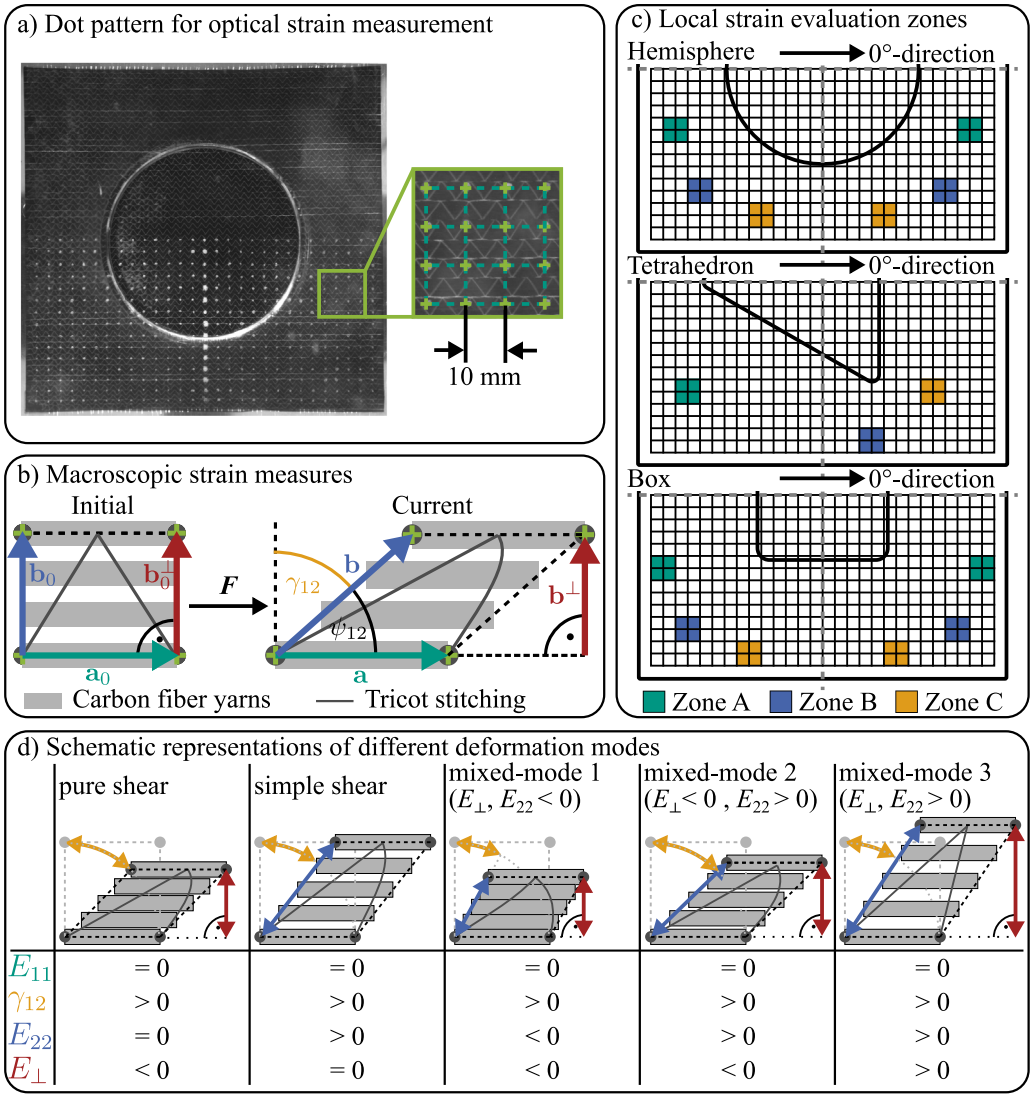

	pure shear	simple shear	mixed-mode 1 ($E_\perp, E_{22} < 0$)	mixed-mode 2 ($E_\perp < 0, E_{22} > 0$)	mixed-mode 3 ($E_\perp, E_{22} > 0$)
E_{11}	$= 0$	$= 0$	$= 0$	$= 0$	$= 0$
γ_{12}	> 0	> 0	> 0	> 0	> 0
E_{22}	$= 0$	> 0	< 0	> 0	> 0
$E_\perp$	< 0	$= 0$	< 0	< 0	> 0

Fig. 4. (a) Dot pattern utilized during 2D-DIC to measure (b) macroscopic strains as well as (c) local evaluation zones for average strains. (d) Schematic representation of different deformation modes, cf. Fig. A.1, and corresponding resulting strains.
Source: Adapted from [38]

between yarns and thus allows identifying gapping ($E_\perp > 0$) as well as perpendicular compression of yarns ($E_\perp < 0$). Thus, it is strongly correlated to the local fiber volume content of the fabric [7]. Positive transverse tensile strains $E_{22} > 0$ indicate large slippage between yarns parallel to each other as well as tension in the stitching direction assuming limited slippage between the stitching and yarns. However, E_{22} does not necessarily indicate gapping, as is evident for example for simple shear or mixed-mode 2 in Fig. 4 d. In many deformation modes observed during the forming tests of this study, the perpendicular and transverse strains have the same sign and allow similar conclusions to be drawn. Thus, the analysis focuses on $E_\perp$ due to its stronger correlation with gapping as well as the fiber volume content, while E_{22} is used to identify zones with significant yarn slippage and compaction (mixed-mode 2).

For a quantitative evaluation of the strain development during the tests, the strains are averaged over three local zones for each shape, cf. Fig. 4 c. The locations of the zones were chosen to reflect the symmetry of each shape, remain in the flat part after the maximum punch displacement, and be positioned in areas of high deformation during forming.

4. Results & discussion

4.1. Outer contours

The resulting outer contours of all tests are shown in Fig. 5. The contours can be used to evaluate the overall deformation behavior [9] and often represent a validation for forming simulation approaches based on the material draw-in [35,36,47]. Furthermore, the fabric after forming consists of one effective zone that represents the desired shape and one non-effective zone that needs to be removed in the subsequent process. Analyzing the outer contour after forming helps in minimizing material waste and production costs during manufacturing.

Single-layer tests. The contour after forming of fabrics usually reflects the symmetry of the utilized shape and material. This results in an orthotropic deformation pattern with fewer symmetries for unbalanced textiles [9,47] compared to balanced fabrics [24,36]. Similar behavior can also be observed for the investigated UD- and Biax-NCF in the single-layer tests shown in the first columns of the respective material in Fig. 5. The Biax-NCF exhibits a nearly balanced structure with a

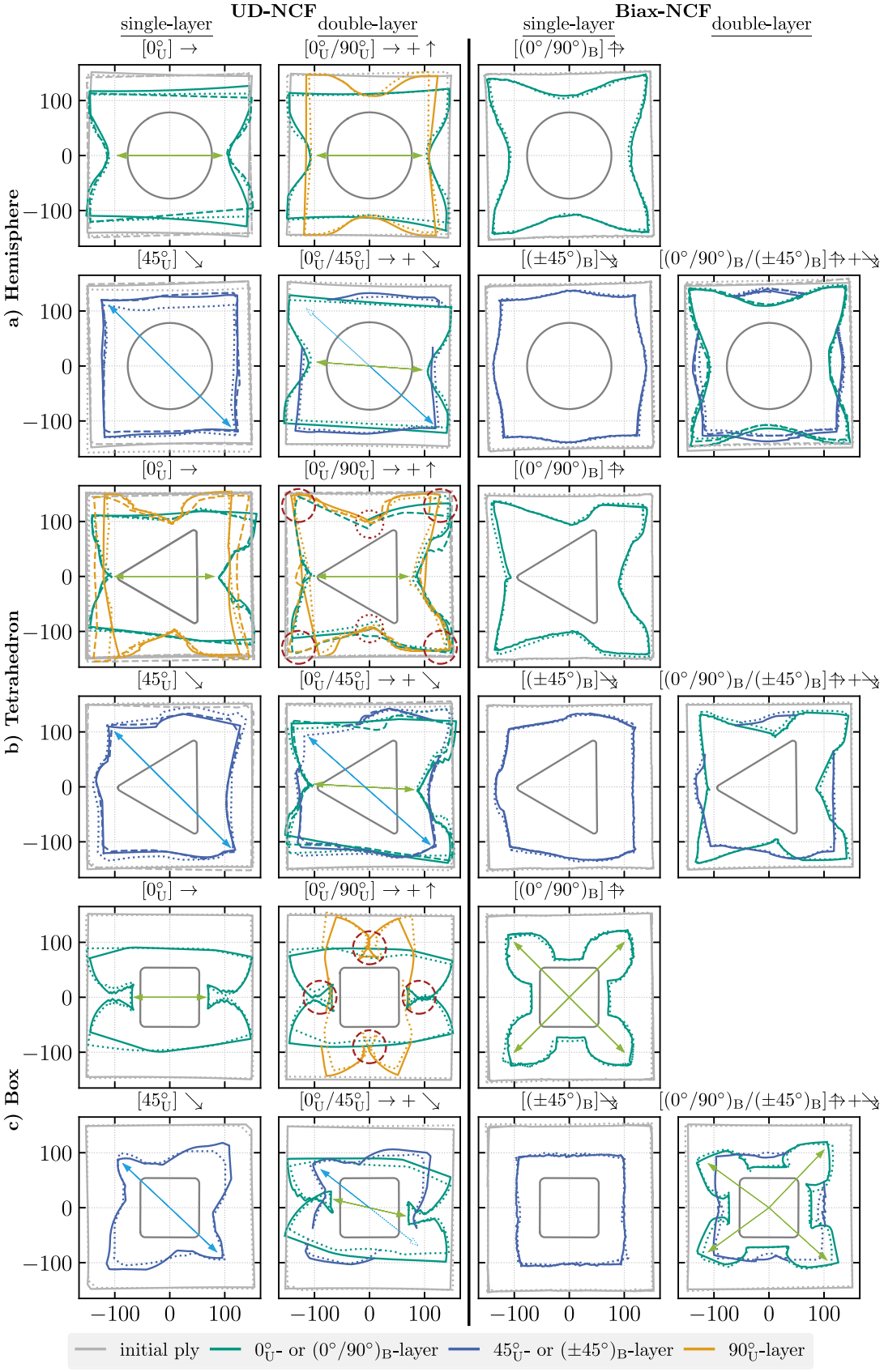

Fig. 5. Outer contours (all in mm) of single- and double-layer configurations in the (a) hemisphere, (b) tetrahedron and (c) box forming tests. Annotations for interactions between layers with arrows and red circles. (For interpretation of the references to color in this figure legend, the reader is referred to the web version of this article.)

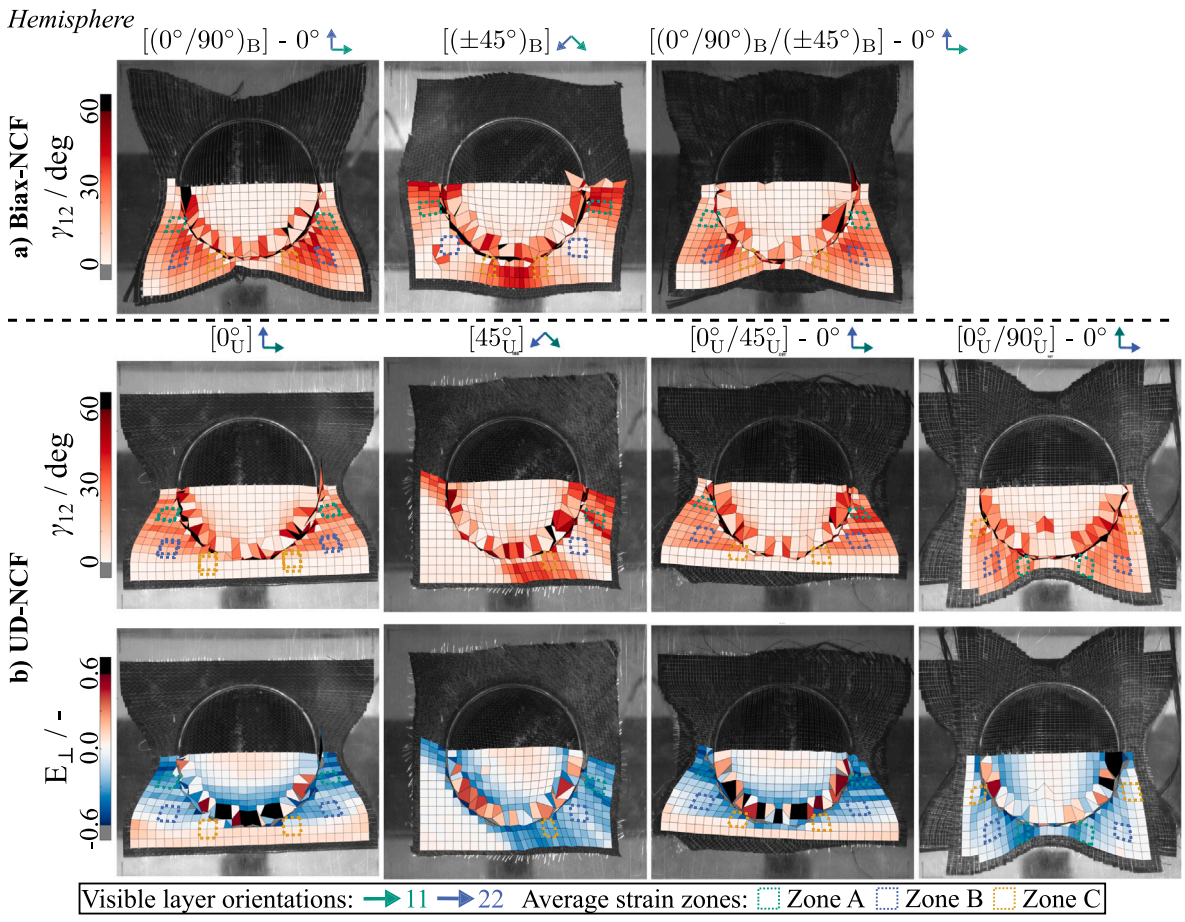

Fig. 6. Most relevant DIC-strain components in the hemisphere shape forming test with different layup orientations at a maximum tool displacement of 75 mm.

symmetrical stitching pattern and a similar number of carbon fibers in both reinforcement directions. Therefore, its highest material draw-in in both fiber directions is close to symmetrical for the point symmetrical hemisphere and box shape, resulting in a quarter-symmetrical contour. In contrast, the highest material draw-in of the very unbalanced UD-NCF has a single preferred direction along the carbon fibers, resulting in a half-symmetrical contour for the hemisphere and box. The tetrahedron has only a single plane of symmetry, so the contours of the Biax-NCF are only half-symmetrical, which is also the case for the UD-NCF in the $[0°_U]$- and $[90°_U]$-tests. The contour of the $[45°_U]$-test of the UD-NCF no longer exhibits any symmetry, because no material axis coincides with a geometric axis of symmetry.

Double-layer tests. The contours of the double-layer tests are shown in the second column of the respective material in Fig. 5 and investigated for a better understanding of the interactions between layers. Significant slippage between the layers can be observed in all tests.

In the *hemisphere* tests, the differences between the individual layers and the respective single-layer tests are quite small, cf. Fig. 5(a). Only in the $[0°_U/45°_U]$-test of UD-NCF the direction of the maximum material draw-in in the fiber direction of both layers tilts slightly (green and cyan arrows) due to the superposition of their mutual deformation. For the Biax-NCF, this rotation is not observed because the deformation of the 45°-layer does not have a single preferred direction. In general, the absence of a binder and relatively low blank holder weight limit the interactions between layers for the hemisphere geometry.

In the $[0°_U/45°_U]$-test on the *tetrahedron* shape, a similar tilt of the draw-in (green and cyan arrows) is observed again only for the UD-NCF, cf. Fig. 5 (b). In the $[0°_U/90°_U]$-test more pronounced interactions between the UD-NCF layers are observed from the contour analysis. The superimposed draw-in of the 90° layer leads to a stronger draw-in of the 0°-layer as indicated by the dotted red circles. Additionally, the corners of the 0°- and 90°-layer remain superposed during some tests (dashed red circles), resulting in a joint deformation of both layers and producing a similar contour to the $[(0°/90°)_B]$-test of the Biax-NCF. The fact that this joint deformation does not always occur is probably caused by the blank holder forces not being large enough to invariably prevent mutual slippage.

For the *square box* shape stronger interactions in the double-layer test are observed, cf. Fig. 5 (c), despite a lower blank holder weight similar to the hemisphere with few significant interactions. The material draw-in of the UD-NCF perpendicular to the fiber direction in the $[0°_U/90°_U]$-test is increased due to the second layer, resulting in partly overlapping flaps of textile (dashed red circles) that were not observed in the single-layer tests. For the Biax-NCF, in the $[(0°/90°)_B/(±45°)_B]$-test a notable tilt of diagonals of the $(0°/90°)_B$-layer due to interaction with the $(±45°)_B$-layer is observed. The increase in interactions for the box shape compared to the hemisphere despite similar blank holder weights, highlights the impact of the more challenging geometry in the context of forming due to the sharp edges and corners instead of a smooth curvature.

Summary. Overall, a significantly larger experimental scatter is observed for the UD-NCF, especially in the direction transverse to the fibers. The deformation in the transverse direction of the UD-NCF is governed by the stitching, which is more compliant and permits larger strains compared to the second fiber direction of the Biax-NCF. Additionally, the stitching pattern is not perfectly homogeneous across each specimen due to the manufacturing process, from which some variation in the material properties is suspected.

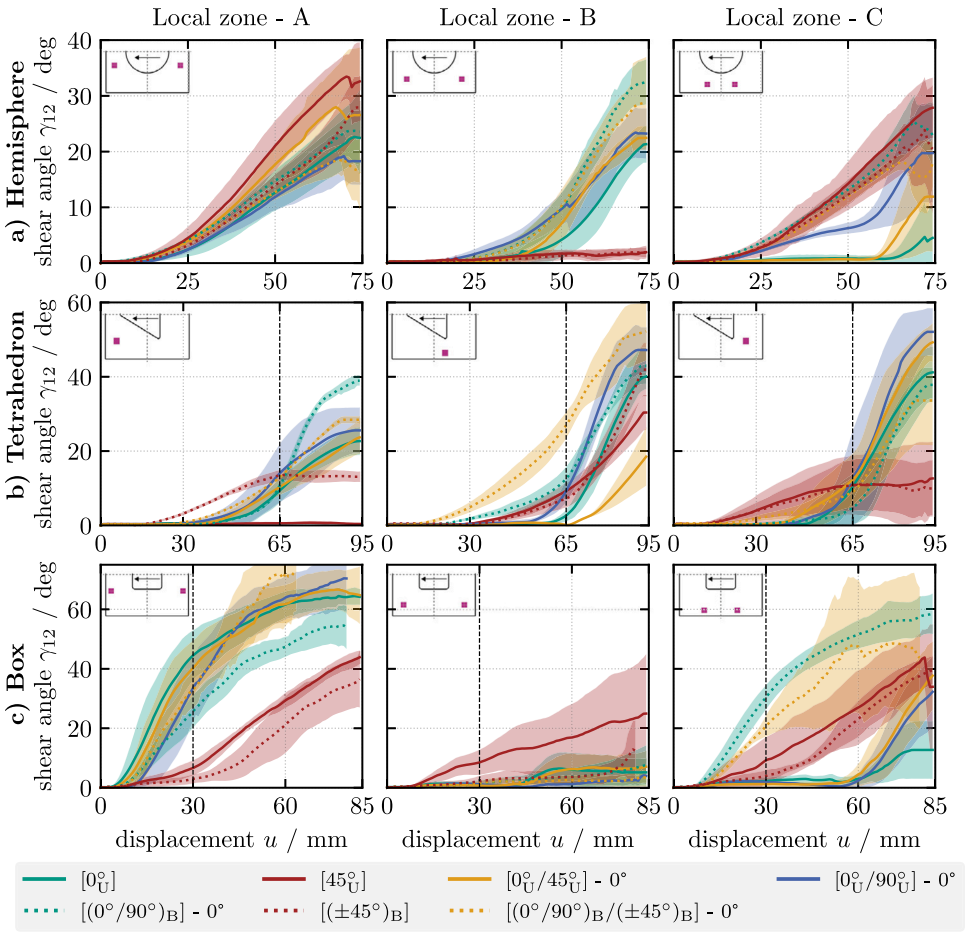

Fig. 7. Local shear angles γ_{12} for the (a) hemisphere, (b) tetrahedron and (c) box punch shapes. The shear is measured on the visible 0°-fiber layer in double-layer setups. Vertical dashed lines indicate geometrical changes in the box and tetrahedron experimental setups. Color bands indicate standard deviation. (For interpretation of the references to color in this figure legend, the reader is referred to the web version of this article.)

In summary, the contours of the single-layer tests are a quantitative measure of the overall deformation of the material. The unidirectional high stiffness of the single fiber direction in a UD-NCF layer is reflected in the resulting contours. The contours of UD-NCF after forming of the different geometries are specific and significantly different from the reported results for other unbalanced fabrics [9,47]. In contrast, the Biax-NCF has a more symmetrical behavior due to the stitching that couples the deformation of both fiber directions within a layer, which results in a behavior similar to balanced woven fabrics [24,36]. The double-layer tests provide insights into the possible interactions between the layers, which depend on the relative orientation between two textile layers, the blank holder weight and the shape of the punch. The double-layer tests of UD-NCF show more signs of mutual interactions in their contour, presumably because of their easier deformability than the Biax-NCF and the more asymmetrical deformation due to the lack of a second fiber direction.

Comparing the $[0°_U/90°_U]$- and $[(0°/90°)_B]$-setup as configurations with an initial 0°- and 90°-fiber layer for both materials, the differences in the forming behavior between UD- and Biax-NCF are most evident. In the hemisphere- and box-test of the UD-NCF, the resulting fiber orientation after forming remains nearly 0°/90° as evident from the outer edges which stay comparably straight due to the independent deformation of the layers. In contrast, the fibers of the Biax-NCF undergo more rotation due to shear in the areas between the bidirectional high material draw-in, because of the coupled deformation of both fiber layers due to the stitching. Only in the tetrahedron test, the stronger interaction between UD-NCF layers due to the higher blank holder forces can result in a joint deformation and the resulting contours are comparable to the Biax-NCF.

4.2. Macroscopic strains

The strains during the tests were measured with DIC based on the method described in Section 3.2. The edges of the openings of the lower dies appear white on the images, with a similar contrast to the white dots of the applied pattern. This results in a loss of correlation for points passing over these edges, which become obvious in strongly deformed elements. The 2D-measurement has the disadvantage that only the strains in the flat area can be measured accurately. In return, the strains can be determined over the entire punch displacement. Furthermore, there is no need for a specialized 3D measuring system, which often requires a way to remove the textile from the mold and is more often used for fabrics with a binder [35,41,48]. The calculated strains in the curved and inclined punch areas are inaccurate due to the neglect of the 3D-geometry. Nevertheless, the measurements of different tests can be qualitatively compared with each other, assuming full contact of the punch with the fabric, which was observed in the closed configurations at maximum punch displacement.

As discussed in Section 3.2, the shear angle γ_{12}, transverse strain E_{22} and perpendicular strain $E_{\perp}$ can be evaluated to distinguish between different deformation modes, cf. Fig. 4 (d). The strains for the different shapes are presented separately depending on their relevance in Figs. 6 & A.2 for the hemisphere, Figs. 8 & A.3 for the tetrahedron and Figs. 9 & A.4 for the square box. The development of the local shear angles in the

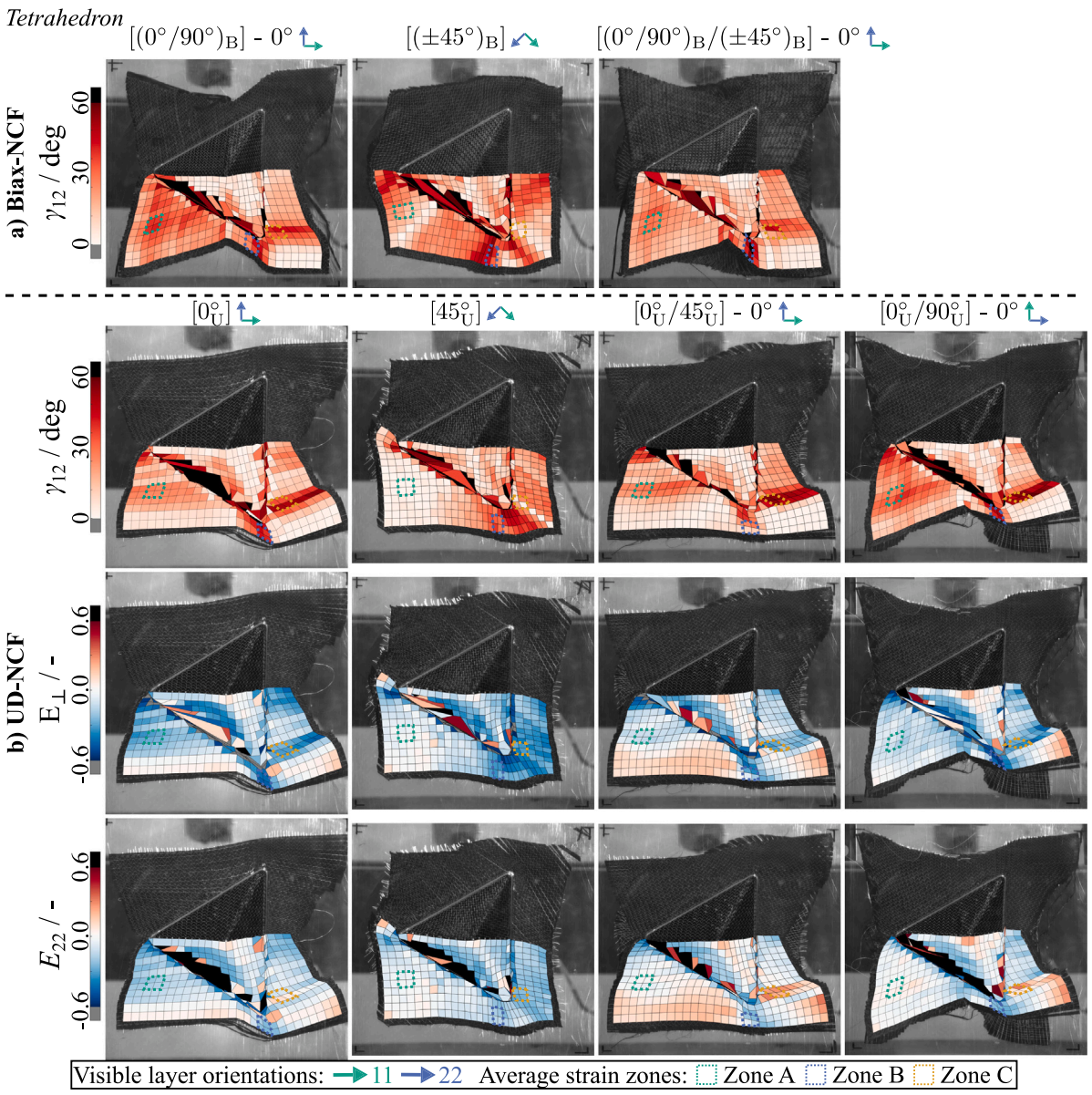

Fig. 8. Most relevant DIC-strain components in the tetrahedron shape forming test with different layup orientations at a maximum tool displacement of 95 mm.

three areas highlighted in Fig. 4 (c) for all three shapes is summarized in Fig. 7.

Hemisphere. First, the most relevant strain components in the hemisphere forming tests are analyzed, which are shown in Fig. 6. The remaining strain components less relevant within the scope of this work are shown in Fig. A.2. For the Biax-NCF, only γ_{12} is presented because mainly shear was observed. The transverse strain E_{22} is close to zero for all configurations, since tension as well as compression is prevented by the second fiber direction, cf. Fig. A.2 a. Thus, the observed compressive strains $E_{\perp}$ result from pure shear, cf. Eq. (2). Both the single- and the double-layer tests with Biax-NCF show a symmetrical shear deformation, cf. Fig. 6 (a), as also evident by development of the local shear angles in Zones A and C, cf. Fig. 7 (a). The additional ±45°-layer in the $[(0°/90°)_B/(\pm45°)_B]$-tests slightly reduces the shear deformation in the visible 0°-layer, cf. Fig. 7 (a). The overall behavior is similar to the results observed for balanced woven fabrics [24,49]. Therefore, the fibers of the Biax-NCF undergo rotation due to the nearly pure shear in the areas between the high material draw-ins in the two fiber directions. No significant yarn slippage was observed, as was found in hemisphere tests by Bel et al. [15] for a similar Biax-NCF with a tricot stitching. This is probably attributable to a higher stitch tension of the Biax-NCF of this study, since local yarn slippage occurred at significantly higher shear angles during characterization in off-axis tensile tests [38].

For the UD-NCF, mainly the mixed deformation modes 1 and 3 (cf. Fig. 4 d) are observed for the hemisphere shape, cf. Fig. 6 (b). Thus, E_{22} is only shown in Fig. A.2 as it has the same sign as $E_{\perp}$, cf. Section 3.2. The UD-NCF has an asymmetric shear behavior with the main deformation due to shear parallel to the fiber direction in all configurations. This is superimposed by perpendicular strains that are not caused by shear alone, as can be concluded by noting that $E_{22} \neq 0$ and has the same sign as $E_{\perp}$. Compared to Biax-NCF, additional tensile and compressive strains in the transverse direction are not prevented by a second fiber direction in each layer. This results in greater in-plane compaction of the fiber yarns in areas of high shear deformation and tension in the stitching direction in areas further away. In the $[0°_U]$-test, positive perpendicular strains are measured in the lower edge regions. Slight gaps between the yarns are visible there and

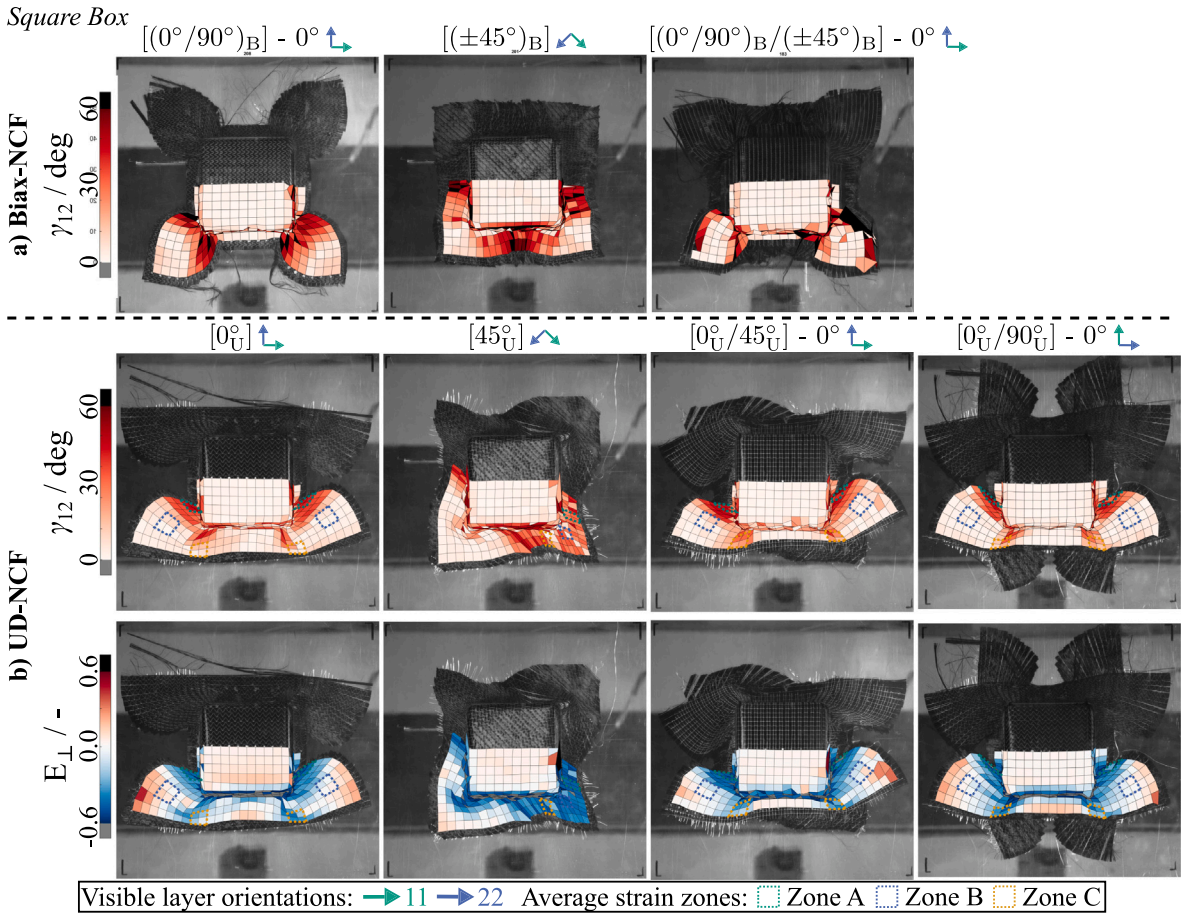

Fig. 9. Most relevant DIC-strain components in the square box shape forming test with different layup orientations at a maximum tool displacement of 85 mm.

the stitching is under high tension. This stitching tension is reduced for the [0°$_U$/45°$_U$]-test and vanishes in the [0°$_U$/90°$_U$]-test, because of the superimposed material draw-in of the second layer. Similarly, positive perpendicular strains are measured for [0°$_U$] and [45°$_U$] in the hemisphere's center despite the distortion caused by the 3D-curvature, but they are reduced in the double-layer tests. The interaction with the superimposed layers increases shear deformation in the areas around zones B and especially C compared to the [0°$_U$]-test, cf. Fig. 7 (a). In zone A, a superposed 90°-layer reduces the shear angle, while a 45°-layer leads to higher shear angles due to the tilted material draw-in, cf. Section 4.1.

Tetrahedron. Second, the most relevant strains components in the tetrahedron forming tests are analyzed, which are shown in Fig. 8 and in Fig. 7 (b). The remaining strain components less relevant within the scope of this work are shown in Fig. A.3. The resulting shear angles close to the corners of the punch are higher than for the hemisphere tests for both materials, due to the small radius of curvature of the tetrahedron in this area. This is especially evident in zones B and C of the 0°-layers in all tests, cf. Fig. 7 (b). For the Biax-NCF, similar to the hemisphere, a nearly symmetric shear-dominated deformation is observed for all configurations, cf. Fig. 8 (a), without notable E_{22}-strains and compressive $E_{\perp}$-strains due to shear. This is similar to the behavior of woven fabrics for this geometry [24].

The main deformation due to shear of the UD-NCF is again observed parallel to the fiber direction, Fig. 8 (b). The shear deformation is superimposed with tensile and compressive strains in mixed-modes 1 and 3 (cf. Fig. 4 d) in most areas. However, comparing the signs of $E_{\perp}$ with E_{22}, mixed-mode 2 is observed in the region around zone C for the 0°-layers of UD-NCF. Notable shear-induced slippage between the fiber yarns occurs in this area, especially in the double-layer tests. In the double-layer tests, the additional 90°-layer also induces a more symmetrical shear behavior in the parts of the 0°-layer remaining superposed during the test, like the lower left half in the [0°$_U$/90°$_U$]-test in Fig. 8(b). This results in a behavior similar to the Biax-NCF and higher shear angles, cf. Fig. 7(b). In the [0°$_U$/45°$_U$]-test, positive perpendicular strains are measured in the lower left edge regions, similar to the observations in the [0°$_U$]-test of the hemisphere. The 45°-layer prevents some of the material draw-in of the 0°-layer resulting in small gaps between the fiber yarns and tension in the stitching.

Square box. Third, the most relevant strain components in the square box forming tests are analyzed, which are shown in Fig. 9 and in Fig. 7 (c). The remaining strain components less relevant within the scope of this work are shown in Fig. A.4. The small radius of the corners and significant depth lead to even higher shear angles than for the tetrahedron shape. The relative observations regarding the measured strains for the tests with the square box shape are similar to those for the hemisphere due to the comparable blank holder weight. The symmetrical shear-dominated deformation without notable yarn slippage of the Biax-NCF is again similar to the behavior observed for balanced woven fabrics [31,32,34]. The UD-NCF mainly deforms under shear (mixed-mode 1, cf. Fig. 4 d) parallel to the fiber yarns with strong strain concentration around the corners of the box. The interactions in double layer tests observed based on the contour, cf. Section 4.1, are only slightly reflected in the locally measured strains. In the area around zone C of the 0°-layers, an increase in the shear angle due to the superimposed layers is measured in the double-layer tests for the UD-NCF, cf. Fig. 7 (c).

Summary. A clear influence of the geometry on the magnitude of the measured strains is obvious. As the complexity and curvature of the

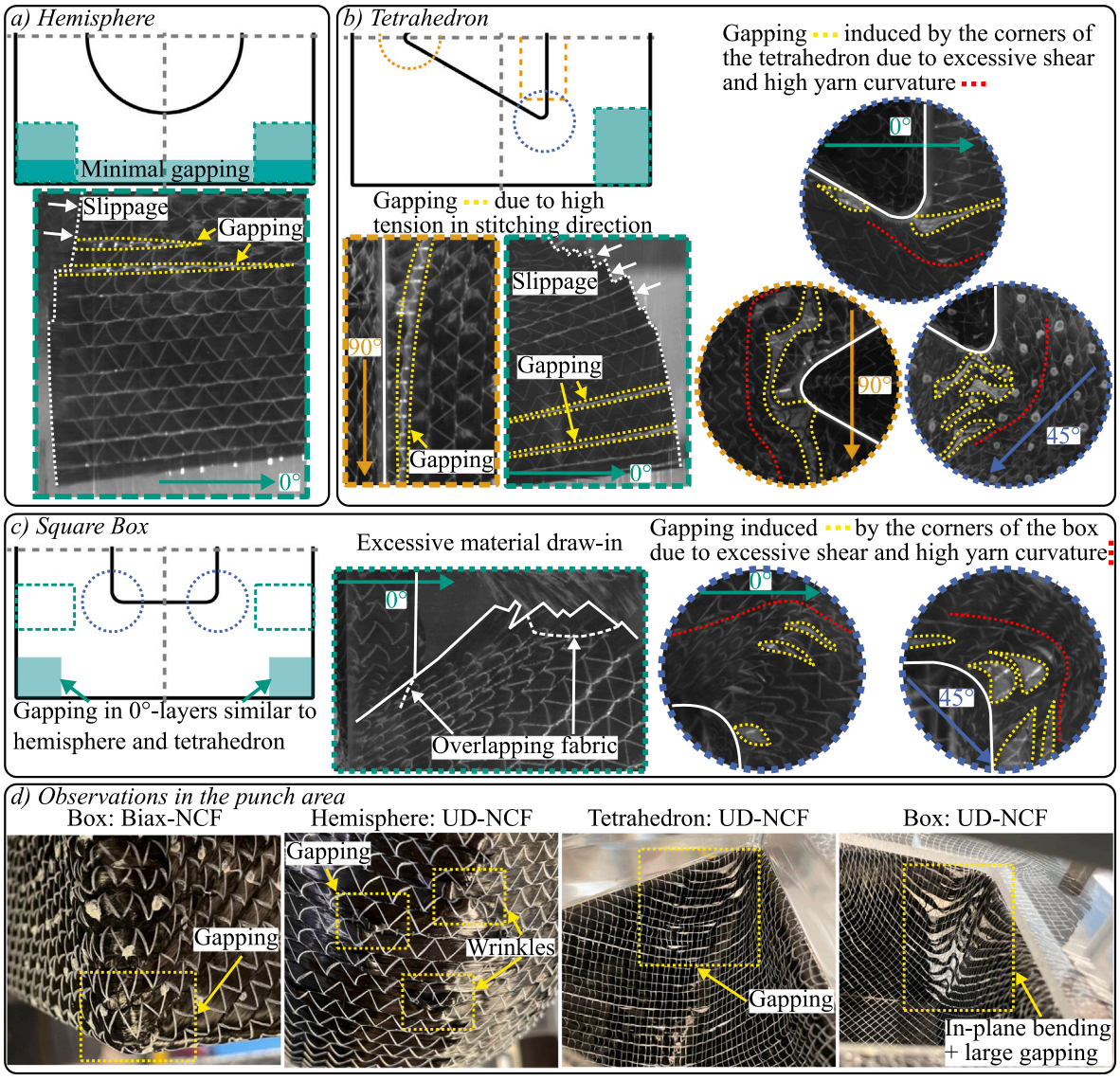

Fig. 10. Schematical overview of the location and type of observed forming effects for the UD-NCF in the planar region for the (a) hemisphere, (b) tetrahedron and (c) square box tests. (d) Additional defects of UD- and Biax-NCF observed in the punch region.

geometry increase from the hemisphere to the tetrahedron to the box, so the measured strains increase too. Especially the forming of the corners of the tetrahedron and box requires a significant material draw-in in those areas, resulting in high strain concentrations. The general difference between the deformation behavior of the nearly balanced Biax-NCF and the highly unbalanced UD-NCF is observed for all shapes.

For the Biax-NCF, the stitching couples the deformation of both fiber layers and prevents notable transverse strains. This results in a main deformation mode of nearly symmetrical shear, similar to balanced woven fabrics. In contrast, the lack of a second fiber direction for UD-NCF results in an asymmetrical shear parallel to the fibers. This is superimposed with additional compressive strains perpendicular to the yarns in areas of high shear and tensile strains due to shear-induced local yarn slippage or stitching tension. Therefore, all deformation modes described in Section 3.2 are relevant for UD-NCF and influence both fiber orientation and fiber volume content, while for Biax-NCF these are mainly influenced by shear. In addition, the forming behavior of UD-NCF is more susceptible to interactions with adjacent layers, with the transverse behavior being particularly affected by superimposed material draw-in.

4.3. Forming defects

Defects may occur during the forming process due to variations in part geometry, reinforcement type, and experimental setup. The applied planar blank holders prevented notable out-of-plane deformation for both NCFs. In the case of Biax-NCF, the structural integrity is enhanced through the two fiber orientations. Only highly localized mesoscopic defects were observed for the Biax-NCF for all investigated shapes. These defects involve isolated gaps and small wrinkles in highly curved areas, such as the corners of the square box shape, as illustrated in Fig. 10 (d).

For the UD-NCF, significantly larger and more systematic defects are detected due to the lower stiffness of the stitching compared to the second fiber direction of the Biax-NCF, cf. Fig. 10. Relative slippage and small gapping between the carbon fiber yarns are visible in the corner areas of the 0°-layers for all shapes (shaded green areas). Defect development was investigated based on the raw images instead of the measured strains due to the limited resolution of DIC, which was necessary to not impact the deformation behavior of the textile [38]. However, areas with gapping coincide with regions of positive perpendicular strains $E_{\perp}$, cf. Section 4.2. Those result from the high tension

in the stitching direction induced by friction with the tools, as well as the largest relative displacements that occur in these areas due to the material draw-in.

Larger gapping is observed near the corners of the punch in the single-layer tests of both the tetrahedron and box shape, cf. circles in Fig. 10 (b) and (c). The localized strong material draw-in in those areas results in high shear deformation, cf. Section 4.2. In cases where the shear cannot propagate parallel to the carbon fibers, the yarns undergo strong in-plane bending deformation (indicated by the red dotted lines). This results in the formation of gaps, which increase in size as the deformation progresses and are also drawn from the flat outer area into the 3D regions, cf. Fig. 10 (d). These gaps develop to a much smaller extent in the double-layer tests, because the superposed layer acts as a reinforcement in the transverse direction and distributes the deformation more evenly.

5. Conclusion

In this study, the forming behavior of a UD- and a Biax-NCF is investigated for different double-curved punch shapes (hemisphere, tetrahedron and square box) and configurations with a focus on the membrane behavior. Transparent tools are combined with an open-source DIC algorithm to allow the analysis of fabrics without binders. A comprehensive analysis is conducted based on the resulting outer contours, macroscopic strains and observed forming defects. The direct comparison of a UD- and Biax-NCF facilitates the identification of their most relevant deformation mechanisms in different forming scenarios.

For the balanced Biax-NCF, the tricot stitching couples the deformation of both fiber layers, and the second fiber direction prevents notable transverse strains. The fibers rotate from their initial orientation due to the nearly pure shear in the areas between the high material draw-ins in the two fiber directions. Thus, the Biax-NCF mainly deforms under symmetrical shear with limited yarn slippage and defects, which is very similar from a macroscopic perspective to the observed behavior of woven fabrics or other balanced NCFs with a symmetrical stitching pattern in literature.

For the highly unbalanced UD-NCF, the lack of a second fiber direction results in an asymmetrical deformation behavior. The fiber orientation after forming often remains similar to the initial orientation because the shear results from parallel yarn slippage. The lower stiffness in the transverse direction leads to additional tensile and compressive strains, which affect the local fiber volume content due to gapping or in-plane yarn compaction. In the single-layer tests in particular, gapping occurs due to large tension in the stitching direction or strong in-plane bending of the yarns since shear transverse to the fiber direction is not possible. The in-plane yarn compaction is an independent deformation component for UD-NCF and is not caused by shear alone, compared to the behavior of balanced fabrics. Thus, the UD-NCF deforms due to shear parallel to the fiber yarns superimposed with significant perpendicular and transverse strains ($E_{\perp}$ and E_{22}) in different mixed deformation modes, which were previously observed during characterization in off-axis tension tests [10,19,38], and measured quantitatively during forming for the first time in this study. To model this specific behavior of UD-NCF in different deformation modes, new approaches are needed that can account for the asymmetric shear behavior and the in-plane bending stiffness of the yarns, which most existing macroscopic approaches based on Cauchy mechanics fail to do.

The relevance of the identified main deformation modes for both NCFs is demonstrated by the observed similarities for the variety of configurations and punch shapes, but only for relatively low blank holder weights. Interactions with adjacent layers can significantly influence the forming behavior, which has a strong influence on the transverse behavior of UD-NCF in particular. Future studies should therefore focus on the influence of the blank holder force on the forming behavior of UD-NCF, which is expected to increase the magnitude of interactions. In addition, the influence of the out-of-plane bending behavior on the deformation modes and the defect formation should be investigated.

The presented results constitute an extensive database to develop and validate forming simulation approaches for UD- and Biax-NCF, which was not available for UD-NCF in particular yet. The data generated in this study is freely available at https://doi.org/10.5281/zenodo.12516897.

CRediT authorship contribution statement

Bastian Schäfer: Writing – original draft, Visualization, Methodology, Investigation, Formal analysis, Conceptualization. **Ruochen Zheng:** Writing – original draft, Methodology, Investigation, Formal analysis, Conceptualization. **Julien Colmars:** Writing – review & editing, Supervision, Methodology. **Auriane Platzer:** Writing – review & editing, Supervision. **Naim Naouar:** Writing – review & editing, Supervision, Project administration. **Philippe Boisse:** Supervision, Project administration, Funding acquisition. **Luise Kärger:** Writing – review & editing, Supervision, Project administration, Methodology, Funding acquisition.

Declaration of competing interest

The authors declare that they have no known competing financial interests or personal relationships that could have appeared to influence the work reported in this paper.

Data availability

The data generated in this study is freely available at

Forming tests of a uni- and a bidirectional non-crimp fabric for different orientations and geometries (hemisphere, tetrahedron, square box) (Original data) (https://zenodo.org/)

Acknowledgments

The authors would like to thank the Deutsche Forschungsgemeinschaft (DFG), Germany and the French National Research Agency (ANR), France for funding the collaborative project "Composite forming simulation for non-crimp fabrics based on generalized continuum approaches" (DFG: 431354059, ANR: ANR-19-CE06-0031), which the presented work is carried out for. This work is also part of the Heisenberg project "Digitalization of fiber-reinforced polymer processes for resource-efficient manufacturing of lightweight components", funded by the DFG, Germany (project no. 455807141)

Appendix

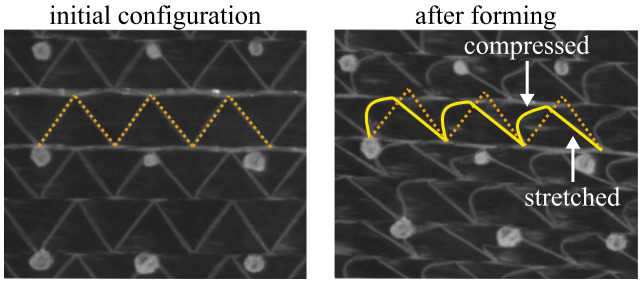

Fig. A.1. Typical stitching deformation with one stretched and one compressed segment.

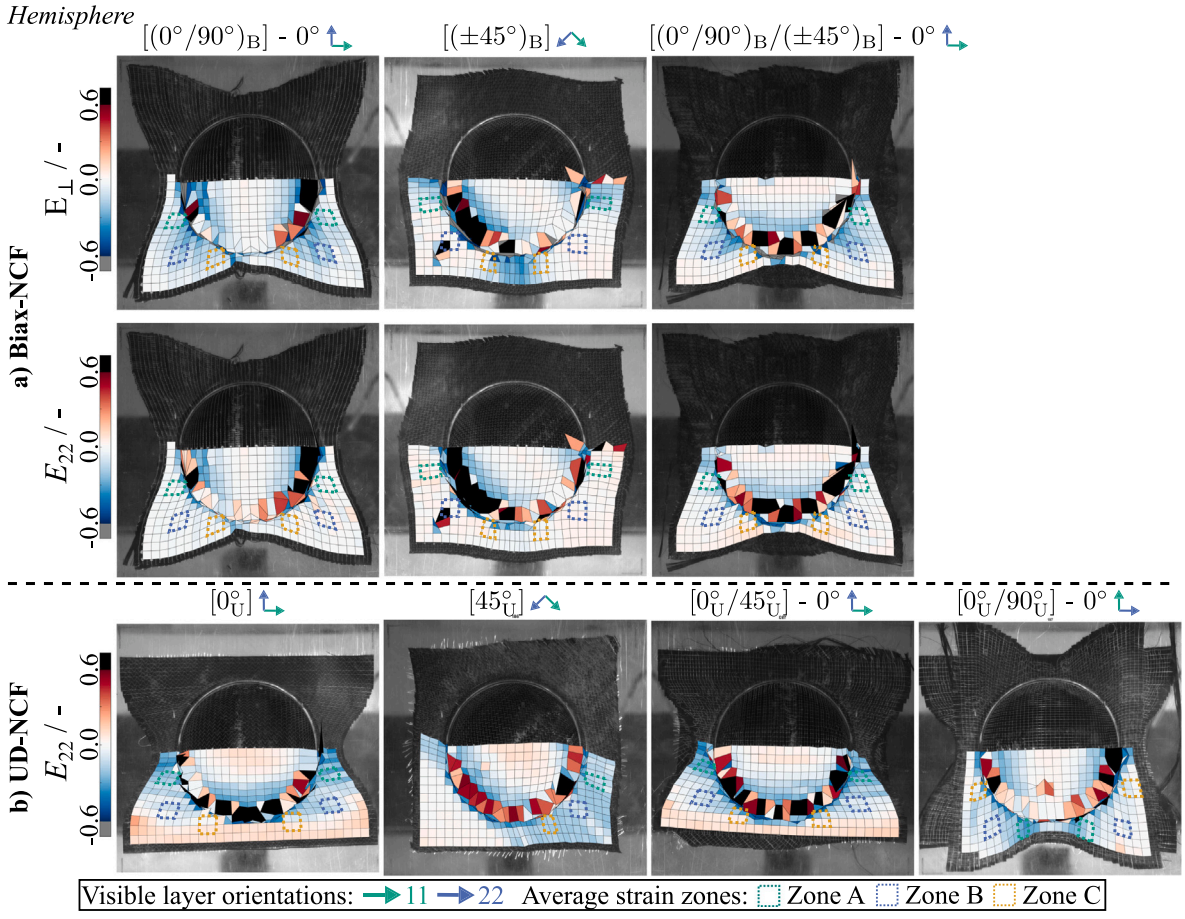

Fig. A.2. Additional DIC-strain components in the hemisphere shape forming test with different layup orientations at a maximum tool displacement of 75 mm.

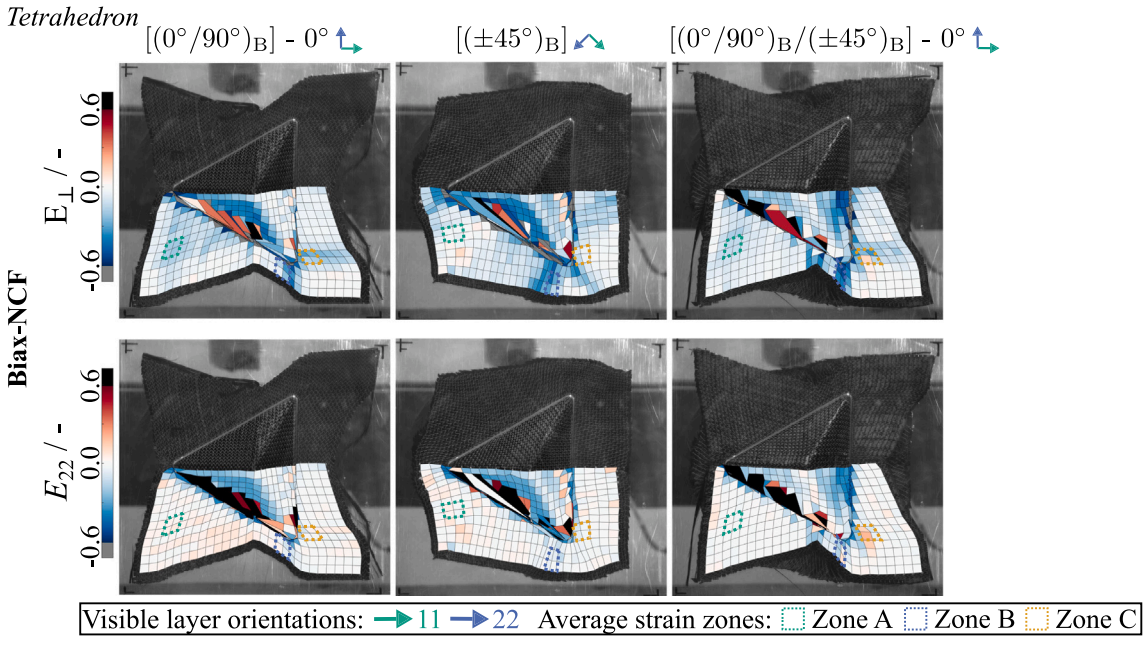

Fig. A.3. Additional DIC-strain components in the tetrahedron shape forming test for UD-NCF with different layup orientations at a maximum tool displacement of 95 mm.

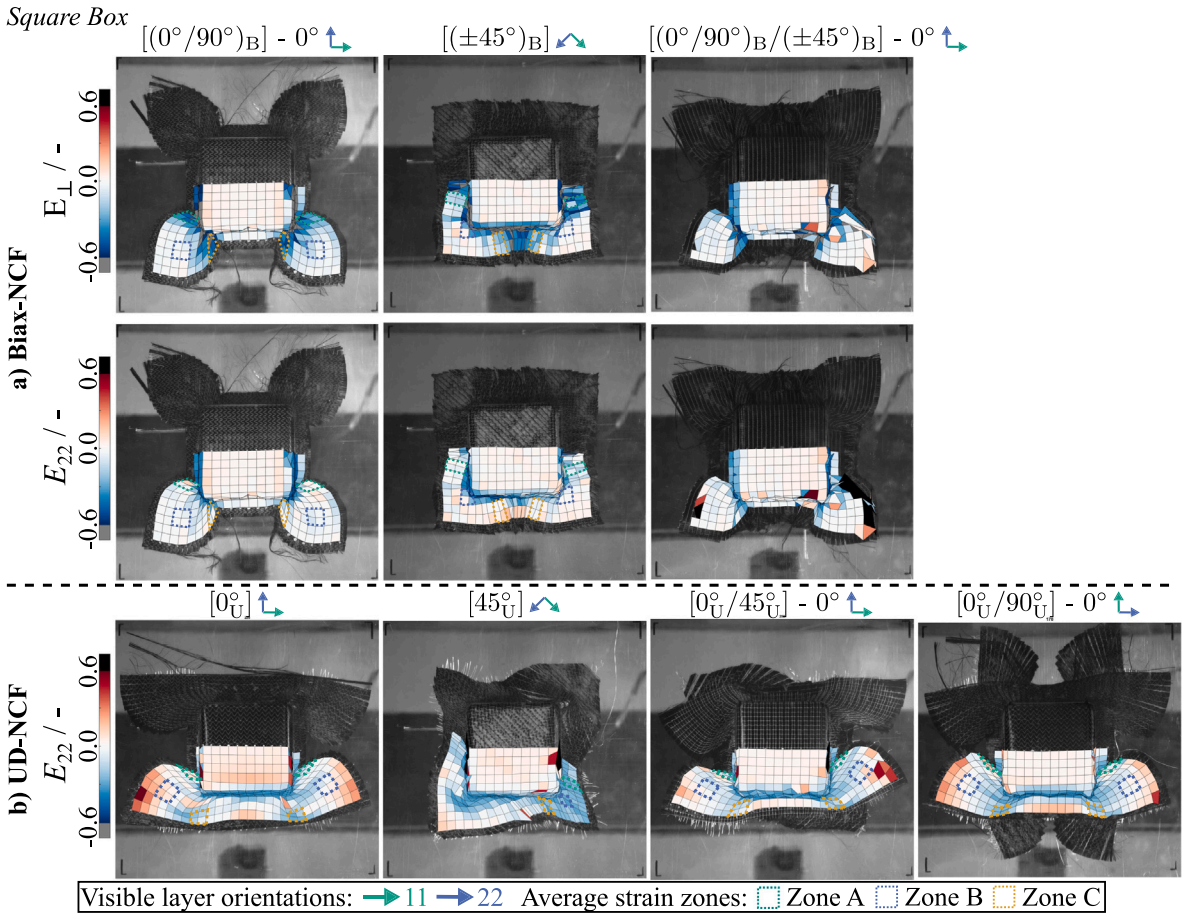

Fig. A.4. Additional DIC-strain components for the box shape forming test for UD-NCF with different layup orientations at a maximum tool displacement of 85 mm.

A.1. Additional macroscopic strain results

Additional results for the macroscopic DIC strains are shown in the following to complete the database for future validation. They are not discussed in more detail, since they would allow for the same conclusions discussed in Section 4.2.

References

[1] Sádaba Sergio, Martínez-Hergueta Francisca, Lopes Cláudio S, Gonzalez Carlos D, LLorca Javier. 10 - virtual testing of impact in fiber reinforced laminates. In: Beaumont PWR, Soutis C, Hodzic A, editors. Structural integrity and durability of advanced composites. Woodhead publishing series in composites science and engineering, Woodhead Publishing; 2015, p. 247–70.

[2] Middendorf P, Metzner C. 18 - aerospace applications of non-crimp fabric composites. In: Lomov Stepan V, editor. Non-crimp fabric composites. Woodhead publishing series in composites science and engineering, Woodhead Publishing; 2011, p. 441–9e.

[3] Sköck-Hartmann B, Gries T. 20 - automotive applications of non-crimp fabric composites. In: Lomov Stepan V, editor. Non-crimp fabric composites. Woodhead publishing series in composites science and engineering, Woodhead Publishing; 2011, p. 461–80.

[4] Deléglise M, Le Grognec P, Binetruy C, Krawczak P, Claude B. Modeling of high speed RTM injection with highly reactive resin with on-line mixing. Composites A 2011;42(10):1390–7.

[5] Sozer EM, Simacek P, Advani SG. 9 - resin transfer molding (RTM) in polymer matrix composites. In: Advani Suresh G, Hsiao Kuang-Ting, editors. Manufacturing techniques for polymer matrix composites (pMCs). Woodhead publishing series in composites science and engineering, Woodhead Publishing; 2012, p. 245–309.

[6] Boisse Philippe, Akkerman Remko, Carlone Pierpaolo, Kärger Luise, Lomov Stepan V, Sherwood James A. Advances in composite forming through 25 years of ESAFORM. Int J Mater Form 2022;15(3):99. http://dx.doi.org/10.1007/s12289-022-01682-8.

[7] Galkin Siegfried, Kunze Eckart, Kärger Luise, Böhm Robert, Gude Maik. Experimental and numerical determination of the local fiber volume content of unidirectional non-crimp fabrics with forming effects. J Compos Sci 2019;3(1). http://dx.doi.org/10.3390/jcs3010019.

[8] Kunze Eckart, Galkin Siegfried, Böhm Robert, Gude Maik, Kärger Luise. The impact of draping effects on the stiffness and failure behavior of unidirectional non-crimp fabric fiber reinforced composites. Materials (Basel, Switzerland) 2020;13(13). http://dx.doi.org/10.3390/ma13132959.

[9] Chuves Yuri Pereira, Pitanga Midori, Grether Inga, Cioffi Maria Odila, Monticeli Francisco. The influence of several carbon fiber architecture on the drapability effect. Textiles 2022;2(3):486–98. http://dx.doi.org/10.3390/textiles2030027.

[10] Ghazimoradi Mehdi, Trejo Eleazar A, Carvelli Valter, Butcher Clifford, Montesano John. Deformation characteristics and formability of a tricot-stitched carbon fiber unidirectional non-crimp fabric. Composites A 2021;82:106366. http://dx.doi.org/10.1016/j.compositesa.2021.106366.

[11] Broberg Peter H, Lindgaard Esben, Krogh Christian, Thompson Adam J, Belnoue Jonathan P-H, Hallett Stephen R, Bak Brian LV. That's how the preform crumples: Wrinkle creation during forming of thick binder-stabilised stacks of non-crimp fabrics. Composites B 2024;273(4):111269. http://dx.doi.org/10.1016/j.compositesb.2024.111269.

[12] Allaoui S, Boisse P, Chatel S, Hamila N, Hivet G, Soulat D, Vidal-Salle E. Experimental and numerical analyses of textile reinforcement forming of a tetrahedral shape. Composites A 2011;42(6):612–22. http://dx.doi.org/10.1016/j.compositesa.2011.02.001.

[13] Bussetta Philippe, Correia Nuno. Numerical forming of continuous fibre reinforced composite material: A review. Composites A 2018;113:12–31. http://dx.doi.org/10.1016/j.compositesa.2018.07.010.

[14] Xie Junbo, Guo Zhenzhen, Shao Mengjie, Zhu Wanqing, Jiao Wei, Yang Zhi, Chen Li. Mechanics of textiles used as composite preforms: A review. Compos. Struct. 2023;304:116401. http://dx.doi.org/10.1016/j.compstruct.2022.116401.

[15] Bel Sylvain, Boisse Philippe, Dumont François. Analyses of the deformation mechanisms of non-crimp fabric composite reinforcements during preforming. Appl Compos Mater 2012;19(3):513–28. http://dx.doi.org/10.1007/s10443-011-9207-x.

[16] Arnold SE, Sutcliffe MPF, Oram WLA. Experimental measurement of wrinkle formation during draping of non-crimp fabric. Composites A 2016;82(3242):159–69. http://dx.doi.org/10.1016/j.compositesa.2015.12.011.

[17] Krieger Helga, Gries Thomas, Stapleton Scott E. Shear and drape behavior of non-crimp fabrics based on stitching geometry. Int J Mater Form 2018;11(5):593–605. http://dx.doi.org/10.1007/s12289-017-1368-1.

[18] Schirmaier FJ, Weidenmann KA, Kärger L, Henning F. Characterisation of the draping behaviour of unidirectional non-crimp fabrics (UD-NCF). Composites A 2016;80:28–38. http://dx.doi.org/10.1016/j.compositesa.2015.10.004.

[19] Schirmaier FJ, Dörr D, Henning F, Kärger L. A macroscopic approach to simulate the forming behaviour of stitched unidirectional non-crimp fabrics (UD-NCF). Composites A 2017;102:322–35. http://dx.doi.org/10.1016/j.compositesa.2017.08.009.

[20] Böhler Patrick, Härtel Frank, Middendorf Peter. Identification of forming limits for unidirectional carbon textiles in reality and mesoscopic simulation. Key Eng Mater 2013;554–557:423–32. http://dx.doi.org/10.4028/www.scientific.net/KEM.554-557.423.

[21] Komeili M, Milani AS. On effect of shear-tension coupling in forming simulation of woven fabric reinforcements. Composites B 2016;99:17–29. http://dx.doi.org/10.1016/j.compositesb.2016.05.004.

[22] Peng Xiongqi, Ding Fangfang. Validation of a non-orthogonal constitutive model for woven composite fabrics via hemispherical stamping simulation. Composites A 2011;42(4):400–7. http://dx.doi.org/10.1016/j.compositesa.2010.12.014.

[23] Chen Bo, Colmars Julien, Naouar Naim, Boisse Philippe. A hypoelastic stress resultant shell approach for simulations of textile composite reinforcement forming. Composites A 2021;149(4):106558. http://dx.doi.org/10.1016/j.compositesa.2021.106558.

[24] Bai R, Colmars J, Chen B, Naouar N, Boisse P. The fibrous shell approach for the simulation of composite draping with a relevant orientation of the normals. Compos Struct 2022;285(8):115202. http://dx.doi.org/10.1016/j.compstruct.2022.115202.

[25] Mei Ming, He Yujia, Yang Xujing, Wei Kai, Qu Zhaoliang, Fang Daining. Shear deformation characteristics and defect evolution of the biaxial ±45° and 0/90° glass non-crimp fabrics. Compos Sci Technol 2020;193(3–4):108137. http://dx.doi.org/10.1016/j.compscitech.2020.108137.

[26] Carvelli Valter, Pazimino Juan, Lomov Stepan V. Formability of a non-crimp 3D orthogonal weave E-glass composite reinforcement. Composites A 2014;61:76–83. http://dx.doi.org/10.1016/j.compositesa.2014.02.004.

[27] Thompson Adam J, Belnoue Jonathan P-H, Hallett Stephen R. Modelling defect formation in textiles during the double diaphragm forming process. Composites B 2020;202(3):108357. http://dx.doi.org/10.1016/j.compositesb.2020.108357.

[28] Viisainen JV, Hosseini A, Sutcliffe MPF. Experimental investigation, using 3D digital image correlation, into the effect of component geometry on the wrinkling behaviour and the wrinkling mechanisms of a biaxial NCF during preforming. Composites A 2021;142(5):106248. http://dx.doi.org/10.1016/j.compositesa.2020.106248.

[29] Danckert Joachim. Experimental investigation of a square-cup deep-drawing process. J Mater Process Technol 1995;50(1):375–84, 2nd International Conference on Numerical Simulation of 3-D Sheet Metal Forming Processes.

[30] Wang Xinyun, Li Jinbo, Deng Lei, Li Jianjun. Metal flow control during hot forming of square cups with local-thickened plates and varied friction conditions. J Mater Process Technol 2018;253:195–203.

[31] Huang J, Boisse P, Hamila N, Gnaba I, Soulat D, Wang P. Experimental and numerical analysis of textile composite draping on a square box. Influence of the weave pattern. Compos Struct 2021;267:113844. http://dx.doi.org/10.1016/j.compstruct.2021.113844.

[32] Wang Peng, Legrand Xavier, Boisse Philippe, Hamila Nahiène, Soulat Damien. Experimental and numerical analyses of manufacturing process of a composite square box part: Comparison between textile reinforcement forming and surface 3D weaving. Composites B 2015;78(9):26–34. http://dx.doi.org/10.1016/j.compositesb.2015.03.072.

[33] Jagpal Rajan, Evangelou Evangelos, Butler Richard, Loukaides Evripides G. Preforming of non-crimp fabrics with distributed magnetic clamping and Bayesian optimisation. J Compos Mater 2022;56(18):2835–54. http://dx.doi.org/10.1177/00219983221103637.

[34] Bai Renzi, Chen Bo, Colmars Julien, Boisse Philippe. Physics-based evaluation of the drapability of textile composite reinforcements. Composites B 2022;242(7):110089. http://dx.doi.org/10.1016/j.compositesb.2022.110089.

[35] Khan MA, Mabrouki T, Vidal-Sallé E, Boisse P. Numerical and experimental analyses of woven composite reinforcement forming using a hypoelastic behaviour. Application to the double dome benchmark. J Mater Process Technol 2010;210(2):378–88. http://dx.doi.org/10.1016/j.jmatprotec.2009.09.027.

[36] Sun Xiaochuan, Belnoue Jonathan P-H, Thompson Adam, Said Bassam El, Hallett Stephen R. Dry textile forming simulations: A benchmarking exercise. Front Mater 2022;9:155. http://dx.doi.org/10.3389/fmats.2022.831820.

[37] Gnaba I, Soulat D, Legrand X, Wang P. Investigation of the formability behaviour during stamping of tufted and un-tufted carbon preforms: towards localized reinforcement technologies. Int J Mater Form 2021;14(6):1337–54. http://dx.doi.org/10.1007/s12289-020-01606-4.

[38] Schäfer Bastian, Zheng Ruochen, Naouar Naim, Kärger Luise. Membrane behavior of uni- and bidirectional non-crimp fabrics in off-axis-tension tests. Int J Mater Form 2023;16(6):68. http://dx.doi.org/10.1007/s12289-023-01792-x.

[39] Lomov Stepan V, Boisse Philippe, De Luycker Emmanuel, Morestin Fabrice, Vanclooster Kristof, Vandeitte Dirk VH, et al. Full-field strain measurements in textile deformability studies. Composites A 2008;39(8):1232–44. http://dx.doi.org/10.1016/j.compositesa.2007.09.014.

[40] Kunze Eckart, Schwarz Benjamin, Weber Tony, Müller Michael, Böhm Robert, Gude Maik. Forming analysis of internal plies of multi-layer unidirectional textile preforms using projectional radiography. Procedia Manufact. 2020;47:17–23. http://dx.doi.org/10.1016/j.promfg.2020.04.110.

[41] Mallach Annegret, Härtel Frank, Heieck Frieder, Fuhr Jan-Philipp, Middendorf Peter, Gude Maik. Experimental comparison of a macroscopic draping simulation for dry non-crimp fabric preforming on a complex geometry by means of optical measurement. J Compos Mater 2017;51(16):2363–75. http://dx.doi.org/10.1177/0021998316670477.

[42] Pazmino Juan, Carvelli Valter, Lomov Stepan V, van Mieghem Bart, Lava Pascal. 3D digital image correlation measurements during shaping of a non-crimp 3D orthogonal woven E-glass reinforcement. Int J Mater Form 2014;7(4):439–46. http://dx.doi.org/10.1007/s12289-013-1139-6.

[43] Eberl Christoph. Digital image correlation and tracking. 2023, MATLAB Central File Exchange URL https://www.mathworks.com/matlabcentral/fileexchange/12413-digital-image-correlation-and-tracking. [Last Accessed 16 January 2023].

[44] Pierce RS, Falzon BG, Thompson MC, Boman R. A low-cost digital image correlation technique for characterising the shear deformation of fabrics for draping studies. Strain 2015;51(3):180–9. http://dx.doi.org/10.1111/str.12131.

[45] Belytschko Ted, Liu Wing Kam, Moran Brian, Elkhodary Khalil I. Nonlinear finite elements for continua and structures. 2nd ed., 1. publ Chichester: Wiley; 2014.

[46] Schäfer Bastian, Dörr Dominik, Zheng Ruochen, Naouar Naim, Kärger Luise. A hyperelastic approach for modeling the membrane behavior in finite element forming simulation of unidirectional non-crimp fabrics (UD-NCF). Composites A 2024;108359. http://dx.doi.org/10.1016/j.compositesa.2024.108359.

[47] Guzman-Maldonado Eduardo, Bel Sylvain, Bloom Dominic, Fideu Paulin, Boisse Philippe. Experimental and numerical analyses of the mechanical behavior during draping of non-orthogonal bi-axial non-crimp fabric composite reinforcements. Mater. Des. 2022;218(3):110682. http://dx.doi.org/10.1016/j.matdes.2022.110682.

[48] Kärger Luise, Galkin Siegfried, Kunze Eckart, Gude Maik, Schäfer Bastian. Prediction of forming effects in UD-NCF by macroscopic forming simulation – Capabilities and limitations. In: Proceedings of the 24th international conference on material forming. 2021, http://dx.doi.org/10.25518/esaform21.355.

[49] Gong Youkun, Yan Dongxiu, Yao Yuan, Wei Ran, Hu Hongling, Xu Peng, Peng Xiongqi. An anisotropic hyperelastic constitutive model with tension–shear coupling for woven composite reinforcements. Int J Appl Mech 2017;09(06):1750083. http://dx.doi.org/10.1142/S1758825117500831.